



Sustainable Degradation of Binary Dye Mixtures Using Fe/Co/rGO Nanocomposite: Dual Dye Dynamics, Adsorption and Reusability

Amina Kanwal¹ · Tayyaba Shahzadi¹ · Tauheeda Riaz¹

Received: 19 January 2024 / Accepted: 5 June 2024
© King Fahd University of Petroleum & Minerals 2024

Abstract

In the present study, rGO was used as supporting material to incorporate Fe/Co nanoparticles to form Fe/Co/rGO composite using aqueous extract of *Dypsis lutescens* leaves. The strong adsorption sites, wide surface areas and oxygen functionalities of reduced graphene oxide (rGO) produced more adsorption and photocatalytic degradation efficiency. Various characterization techniques like UV–visible spectrophotometer, FTIR, XRD, EDX and SEM were performed to analyze the synthesized nanocomposite, which confirmed the crystalline, porous nature of nanocomposite with average size of 5 nm. Degradation mechanism of mixture of cationic (rhodamine B) and anionic (alizarin red) dyes was observed with and without tungsten lamp source. Different parameters (time, pH, dye concentration, Fe/Co/rGO dosage and temperature) affecting adsorption and degradation of dyes were examined. At 5 ppm dyes solution and 10 mg nanocatalyst dosage in time limit of 20 min, without tungsten lamp, % removal of rhodamine B was observed as 62% and that of alizarin R was 59%, while under tungsten lamp % removal was increased upto 95% for rhodamine B and 90% for alizarin R. Kinetics of adsorption mechanism revealed that process followed pseudo-2nd-order reaction. Thermodynamic studies predicted that adsorption process was spontaneous and exothermic in nature. Among different isotherm models applied, the Freundlich isotherm model was best fitted. Moreover, the reusability studied showed that nanocatalyst is effective even after five cycles and hydroxyl radicals were the main specie of degradation mechanism.

Keywords Fe,Co-rGO nanocomposite · Rhodamin B and alizarin red dyes · Adsorption–photodegradation · Kinetics & thermodynamic studies

1 Introduction

Clean water is significant for all types of flora and fauna. It is a natural resource of life, but unfortunately due to human activities including population growth and increased number of industries, this natural resource is being destroyed. Various organic and inorganic contaminants are polluting the water resources. Dyes effluents coming from leather, textile and other related industries are dangerous for the environment because of their toxic nature. The presence of dyes in wastewater has become a severe concern. Dyes are the second largest pollutants in the wastewater. It is the need of time to treat wastewater before releasing into the environment. Dyes are the natural or synthetic substances that are being used to

impart colors in different industries like paper, leather and textile, etc. Nowadays, more than 9000 dyes are being used in different industries [1, 2]. Despite the advantages of dyes, their elimination into the water can cause hazardous environmental issues because nearly all of the dyes which are being used are lethal and a few are carcinogenic and mutagenic for human beings [3, 4]. Dyes are the major pollutants for aquatic life because they produce toxic materials on degradation. The degraded products impart unwanted color in water, stop the sunlight penetration and cause higher level of BOD and COD [5]. Hence, it is a substantial issue that has been spoken by numerous researchers to find a maintainable treatment method.

Rhodamine B is a synthetic cationic dye having pink color, used in dyeing industries and for printing tasks, but it can be harmful to eyes, skin and nervous system, while alizarin red is a synthetic anionic dye having red color, used for textile industries and to stain biological specimens [6, 7]. Dyes are stable to the biodegradation, photodegradation, heat and

✉ Tayyaba Shahzadi
tayyaba332@gmail.com; tayyaba.shehzadi@gcwus.edu.pk

¹ Department of Chemistry, Government College for Women University Sialkot, Sialkot 51310, Pakistan



oxidizing agents because of their synthetic origin and intricate aromatic structures. Therefore, various methodologies are adopted to eliminate dyes like flocculation, coagulation, membrane filtration, chemical reduction, degradation, electrochemical techniques, anaerobic or aerobic treatments and adsorption [8–10]. Adsorption is considered to be the best method for dyes removal from aquatic effluents due to its low cost, high efficiency and ease to work [11, 12]. Among different approaches, nanotechnology has emerged as a promising approach to treat wastewater without posing threat to environment. Nanocomposites have gathered attention of researchers because of their high potential to remove pollutants from aquatic system. Reduced graphene oxide is a derivative of graphene having 2D structure that shows synergistic effect when used as a matrix for metallic nanoparticles. Graphene composites have excellent features like greater surface area and higher pore volume [13–15].

In this research work, graphene was used as a supporting material to synthesize Fe/Co/rGO nanocomposites by addition of metals in a single step, which was further used to remove dyes from aqueous media. Different factors were optimized during adsorption mechanism for maximum removal of cationic and anionic dyes from aqueous media. Thermodynamics, kinetic studies and different adsorption models were applied on adsorption mechanism. To analyze the efficiency of synthesized nanocomposite, reusability was also examined.

2 Material and Methods

2.1 Materials

Throughout this experimental work, analytical grade chemicals were used, i.e., iron sulfate (FeSO_4), cobalt chloride ($\text{CoCl}_2 \cdot 6\text{H}_2\text{O}$), graphite powder, potassium permanganate (KMnO_4), sulfuric acid (H_2SO_4), hydrogen peroxide (H_2O_2), alizarin R dye and rhodamine B dye.

2.2 Preparation of Plant Extract

The leaves of the plant were carefully washed and left to dry in the shade. Once dried, the leaves were transformed into a fine powder. Subsequently, 3 g of the powdered leaves was mixed with 100 mL of distilled water and subjected to boil at a temperature of 70 °C for duration of 45 min. Afterward, the aqueous extract was allowed to cool down to room temperature and then filtered. The resulting filtrate was then stored at room temperature and used in subsequent experiments [16].

2.3 Fabrication of Graphene Oxide (GO)

Graphene oxide was synthesized from graphite powder using a modified Hummer's method. To initiate the process, 1 g of graphite powder was introduced to a 25 mL of sulfuric acid (H_2SO_4) in beaker, while vigorously stirring the mixture in an ice bath. Subsequently, 3 g of potassium permanganate (KMnO_4) was gradually added to the reaction mixture. The stirring continued for 3 h, after which 50 mL of distilled water was carefully added drop by drop, maintaining the temperature below 50 °C.

To further facilitate the reaction, an instant addition of 100 mL of distilled water was made to the reaction medium. In order to halt the reaction and precipitate any unreacted MnO_4^- ions into MnO_2 , 5 mL of hydrogen peroxide (H_2O_2) was added. To eliminate excess acid, the resulting mixture underwent multiple washes with distilled water and was subsequently centrifuged to obtain the residual product. The solid product was then dehydrated by placing it in an oven set at 60 °C for duration of 24 h [17–19].

2.4 Preparation of Fe/Co/ rGO Composites

In the preparation of Fe/Co/rGO composites, a 100 mL of plant extract was added to 1.0 g of graphene oxide (GO) in beaker. The mixture was subjected to continuous stirring for duration of 10 min. Following this, 20 mL of a solution containing FeSO_4 (0.05 M) and an equal amount of CoCl_2 (0.05 M) was introduced into the reaction mixture. To promote the desired reaction, the mixture was maintained at a temperature of 80 °C and subjected to vigorous stirring for a period of 8 h [20].

2.5 Characterization Techniques

To explore the dimensions, arrangement and physical characteristics of the synthesized nanocomposite, various characterization techniques were employed. These techniques included UV–Vis spectrophotometer (Specord 210 Plus, Analytik Jena AG, Germany), scanning electron microscopy (SEM), X-ray diffraction (JEOL, Neoscope, JCM-600), energy-dispersive X-ray spectroscopy (Vega LMU, TESCAN, Czech Republic) and Fourier transform infrared spectroscopy (Thermo Scientific Nicolet 6700). By utilizing these methods, a comprehensive analysis of the size, structure and morphology of the nanocomposite was conducted.

2.6 Dyes Adsorption

In the adsorption experiments, two dyes, Rhodamine B and Alizarin R, were employed. A stock solution with a concentration of 1000 ppm was prepared for each dye. From the stock solution, different concentrations, specifically 5 ppm,

25 ppm, 75 ppm and 100 ppm, were prepared by dilution. Furthermore, equal concentrations of both dye solutions were combined to create a binary system of dyes.

To determine the maximum capacity of the synthesized nanocomposite for dyes removal, various factors such as pH, adsorbent dosage, dye concentration, contact time and temperature were optimized. This optimization process aimed to identify the ideal conditions that would yield the most efficient and effective removal of dyes using the nanocomposite.

2.7 Point of Zero Charge

25 mL of 0.1 M NaNO₃ solution was taken in different beakers, and to adjust the pH values, the appropriate amount of either 0.1 M HCl or 0.1 M NaOH was added to each beaker containing the NaNO₃ solution. Subsequently, 10 mg of the adsorbent material was introduced into these pH-adjusted beakers and left undisturbed for approximately 24 h on an orbital shaker. After the 24-h duration, the final pH (pH_f) was determined.

To determine the point of zero charge, a graph was created by plotting a straight line between the initial pH values (pH_i) and the difference in pH (ΔpH or pH_i–pH_f). This graph provided valuable insights into the point at which the adsorbent material exhibited no net charge [21–23].

2.8 Thermodynamics Studies

Thermodynamic parameters were calculated through optimization of temperature during adsorption. Following equation was used for thermodynamic parameters

$$\ln K_d = \frac{\Delta S^\circ}{R} - \frac{\Delta H^\circ}{RT} \tag{1}$$

Here, ΔH° represents the change in enthalpy, ΔS° denotes change in entropy, R is the general gas constant, and T is the temperature in kelvin (K). K_d represents the distribution coefficient and is calculated from

$$K_d = \frac{q_e}{C_e} \tag{2}$$

Gibbs free energy (ΔG°) was also calculated through following equation

$$\Delta G^\circ = -RT \ln K_d \tag{3}$$

2.9 Adsorption Kinetics Models

Adsorption kinetics of dyes on synthesized nanocatalyst was investigated by pseudo-1st order (PFO) and pseudo-2nd order (PSO).

Following mathematical Eqs. 1 & 2 were used for the calculations of these models, respectively.

$$\ln(q_e - q_t) = \ln q_e - k_1 t \tag{4}$$

$$\frac{t}{q_t} = \frac{1}{k_2 q_e^2} + \frac{t}{q_e} \tag{5}$$

In both equations q_e is removal capacity constant at equilibrium and q_t is adsorption constant at different time intervals. Rate constant is denoted by K₁ for PFO and K₂ for PSO.

2.9.1 Adsorption Isotherms

To investigate adsorption process three isotherms were applied, i.e., Langmuir, Freundlich and Temkin isotherm.

Actually Freundlich isotherm concerned about multilayer adsorption and heterogeneous distribution of dye molecules on nanocatalyst surface. Freundlich equation of adsorption isotherm was used here:

$$\log K_e = \log K_{f+1/n} \log C_e \tag{6}$$

K_f is adsorption capacity and 1/n is adsorption intensity. Equation of Langmuir adsorption isotherm was following

$$\frac{1}{q_e} = \frac{1}{K_L q_m} * \frac{1}{C_e} + \frac{1}{q_m} \tag{7}$$

Here, q_m is the adsorption constant.

Another isotherm Temkin was applied on experimental data. This isotherm was related to changes in heat during adsorption. Following Temkin equation was used

$$q_e = \frac{RT}{B \ln(k_T)} + \frac{RT}{B \ln(C_e)} \tag{8}$$

K_T is the Temkin constant that provides information about binding energy of dye molecules on nanocatalyst. B_T gives information about heat of adsorption.

3 Results and Discussion

3.1 XRD Analysis

The XRD pattern of graphene oxide (GO) is shown in Fig. 1a. A wide diffracted peak between 10° and 20° was observed that confirmed the GO structure having vertical oxides of graphite. Further small peaks at 30°, 40° and 50° were seen that give information about incomplete interconnection of graphene oxide with oxygen atoms. More regular structure of graphene oxide observed after reduction of graphene oxide

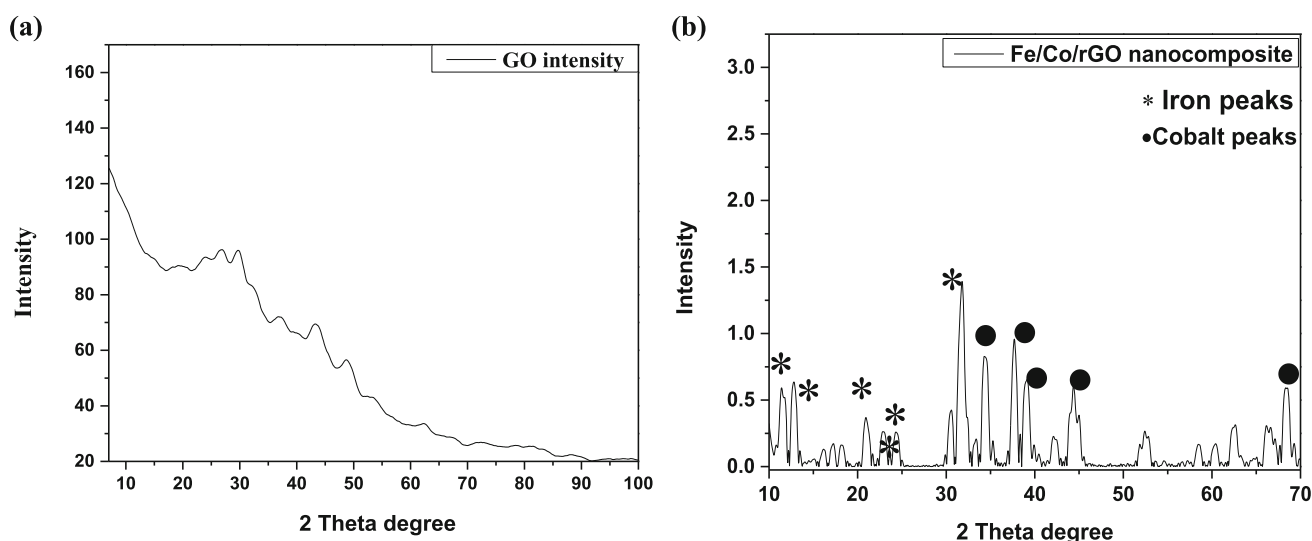


Fig. 1 a XRD image of GO b XRD image of Fe/Co/rGO nanocomposite

with plant extract to form graphene-based nanocomposite [24]. To calculate the crystalline size of synthesized nanomaterial X-ray diffraction technique was performed. XRD spectra of synthesized nanocomposite (Fe/Co/rGO) showed peaks at 11° , 13° , 20° , 23° , 24° , 30° , 31° , 34° , 37° , 38° , 42° , 44° , 52° , 58° , 62° , 66° , 68° (Fig. 1b). Ten Bragg angles were observed between 0 and 100 diffracted intensities [25]. Peaks at lower intensities at 2θ values 10° to 30° were observed due to iron moieties, and at higher intensities peaks having 2θ values 30° to 60° due to cobalt elements were detected. These data were used to find out the average size of nanocomposite, which was 5 nm, calculated through Debye–Scherrer equation.

$$D = (k\lambda / \beta \cos \theta) \quad (9)$$

Constants of this equation denote.

K (proportionality constant) = 0.9

λ = wavelength of X-rays.

β = Full width at half maximum (FWHM).

3.2 Scanning Electron Microscopy (SEM)

SEM images were captured at different magnifications as shown in Fig. 2. Basically, scanning electron microscopy describes about the morphology and crystalline nature of synthesized nanomaterial. Here at 500 nm granular and sphere structure of nanocomposites can be seen, while in the images $1 \mu\text{m}$, $2 \mu\text{m}$ and $5 \mu\text{m}$ some assemblages of particles can be detected. Clusters and agglomeration of material indicate that nanomaterial is polymeric in nature. Another characteristic of the material is its porous nature that will be an excellent property toward adsorption [26]. As the synthesized material Fe/Co/rGO was used for adsorption of dyes, hence its

porous structure will made it more compatible for effective adsorption mechanism.

3.3 Energy-Dispersive X-ray (EDX)

Energy-dispersive X-ray spectroscopy is performed to analyze the purity of synthesized material, and elemental composition is also described. Fe/Co/rGO was characterized to look into its basic composition. It can be seen that Fe, Co, C and O were present in the synthesized Fe/Co/rGO composite (Fig. 3). All these elements were used to synthesize the required material; therefore, it was concluded that no other impurities are present in EDX spectrum [27].

3.4 Fourier Transforms Infrared (FTIR) Analysis

Fourier transform infrared method is used to detect changes in composition of material due to changings of functional groups. A particular wavelength of infrared radiation due to rotational and vibrational movement of molecules is detected by FTIR. Thus structural differences can be seen due to molecular binding of different moieties. In the following spectrum of GO and Fe/Co/rGO nanocomposites peaks of different functional groups can be seen between 500 and 4000 cm^{-1} . In the FTIR spectrum of GO due to extensive oxidation stretching vibrations of OH at 2988 cm^{-1} , C = O at 1541 cm^{-1} , C–O at 1575 cm^{-1} and OH deformation vibration bond at 697 cm^{-1} were observed (Fig. 4a).

Due to reduction reaction of Fe/Co/rGO nanocomposite the above peaks are relatively weak or completely removed in the FTIR spectra of synthesized nanocomposite (Fig. 4b). Broad and strong stretching vibrational peak of OH can be observed at 3165 cm^{-1} and 2164 cm^{-1} . Carboxyl group

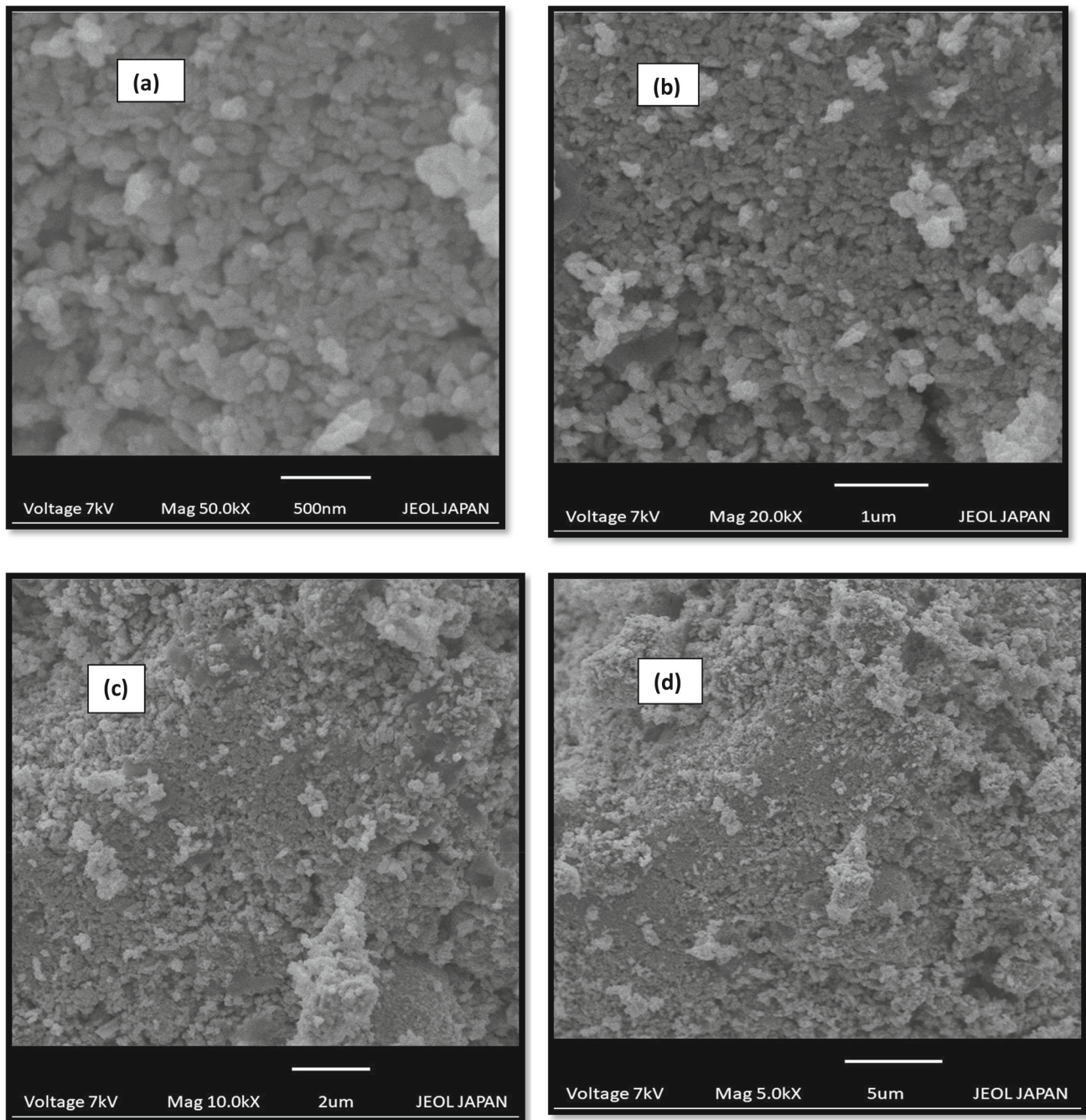


Fig. 2 SEM photographs of Fe/Co/rGO nanocomposite at different resolution of 500 nm, 1 μm , 2 μm and 5 μm

(C = O) stretching band at 1614 cm^{-1} , carbonyl group (C=O) stretching band at 1358 cm^{-1} and vibrational bands at 972 cm^{-1} , 741 cm^{-1} are present in the FTIR spectrum of Fe/Co/rGO nanocomposite [28]. It was observed that after reduction, some peaks of GO were disappeared and others appeared with noticeably reduced intensities.

3.5 UV-Visible Spectroscopy

UV-visible spectroscopy is performed to confirm the synthesis of nanomaterial. An obtained spectrum depicts a peak between 180 and 250 nm that inveterate the synthesis of Fe/Co/rGO nanocomposite. To confirm the synthesis of nanomaterial, its spectrum was compared with the spectrum of GO (Fig. 5a). Herein characteristic peaks appeared at 210 nm and 300 nm in spectrum of GO with band gap

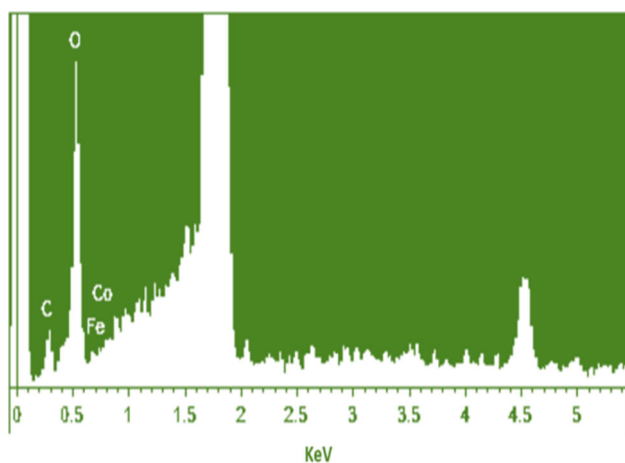


Fig. 3 EDX spectrum of Fe/Co/rGO nanocomposite

energy of 4.3 eV (Fig. 5b). The $\pi \rightarrow \pi^*$ transition of C = C bonds for GO was found at 233 nm. A peak at 300 nm showed C = O carbonyl functional group of GO due to $n \rightarrow \pi^*$ transition. A broad peak at 180–250 nm in spectrum of Fe/Co/rGO nanocomposite depicted the fine deposition of Fe/Co on surface of rGO. Shifting of the peak toward lower

wavelength also confirmed the synthesis of nanocomposite [29]. The Tauc and Davis–Mott relation was used to calculate energy band gap of the GO and nanocomposite.

$$(\alpha h\nu)^n = K(h\nu - E_g) \quad (10)$$

where K is energy independent constant, $h\nu$ is the incident photon energy, α is absorption coefficient, n is the nature of transition, and E_g is the band gap energy.

Band gap energy calculated for synthesized GO and Fe/Co/rGO nanocomposite was found to be 4.3 eV and 3.02 eV, respectively (Fig. 5b and c).

3.6 Point of Zero Charge

To study the adsorption mechanism point of zero charge calculation is very important because adsorption depends upon the surface charge of adsorbent. To calculate the net charge on surface, salt addition method was used here. The calculated size of synthesized Fe/Co/rGO nanocomposite was 6.65 as shown in Fig. 5d. Surface of adsorbent can be made more compatible to remove cationic and anionic dyes. Pzc plays an important role to create charge on surface as higher pH

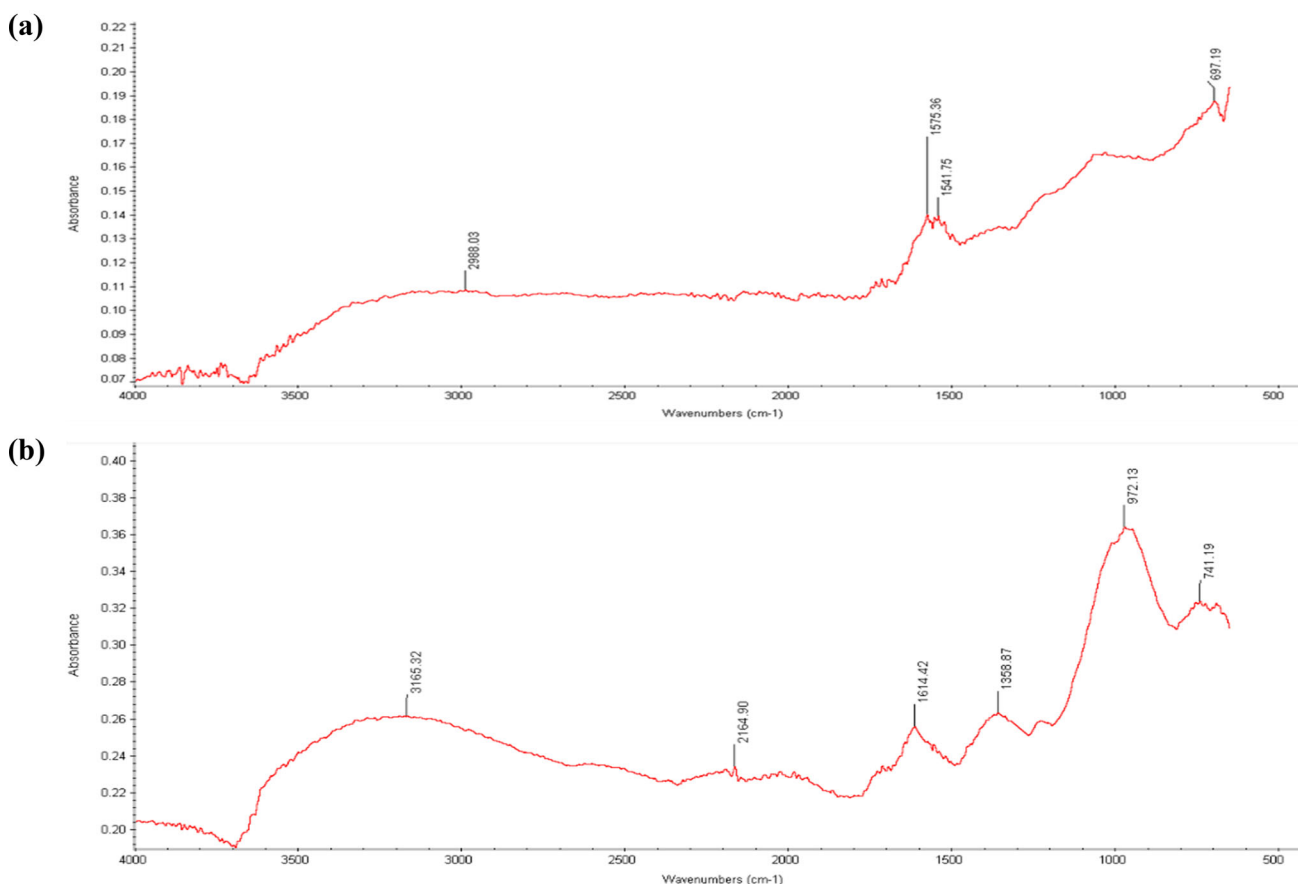


Fig. 4 a FTIR spectrum of GO b FTIR spectrum of Fe/Co/rGO composite

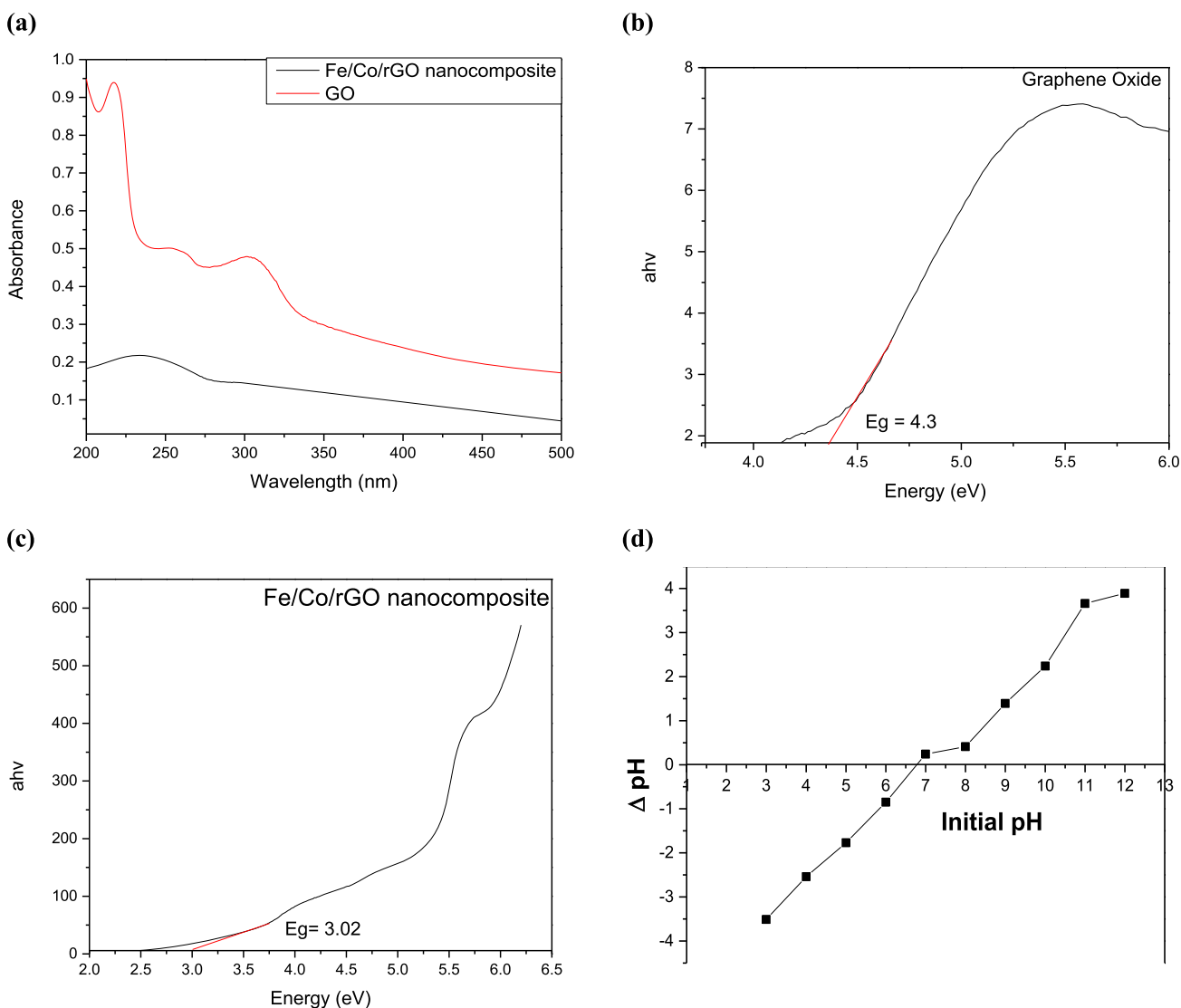


Fig. 5 a Comparative UV–visible spectrum of Fe/Co/rGO nanocomposite and GO b Energy band gap of synthesized GO. c Energy band gap of synthesized Fe/Co/rGO nanocomposite d Point of zero charge calculation of Fe/Co/rGO nanocomposite

value will lead to negative charge on the surface and lower pH value will lead to positive charge on the adsorbent surface.

3.7 Adsorption Studies of Dyes

Following factors were optimized for maximum adsorption of dyes from binary mixture onto surface of Fe/Co/rGO nanocatalyst.

3.7.1 Effect of Dye Concentration

To optimize the factor of dye concentration different binary solutions of both dyes (5 mg/L, 10 mg/L, 25 mg/L, 75 mg/L, 100 mg/L) were prepared and then 10 mg of the Fe/Co/rGO nanocatalyst was added to the 25 mL of each binary solution

of dye. Reaction time was set for about 2 h with continuous stirring on orbital shaker. It can be seen from Fig. 6a and b that with increasing dye concentration dye removal percentage was decreased. Reason behind this decrease of % dye removal was establishing equilibrium and formation of monolayer. Moreover upon increasing dye concentration, active sites of the adsorbent material decreased. At lower dye concentration, i.e., 5 mg/L, maximum % removal of dyes was observed. Optimization of the factor was achieved once under tungsten lamp and then without using tungsten lamp. Without tungsten light source, % removal of dyes was 62% for rhodamine and 59% for alizarin dye. The identical experiment was carried out with a tungsten light source, and % removal of dyes was increased upto 95% for rhodamine and 92% for alizarin dye [30, 31]

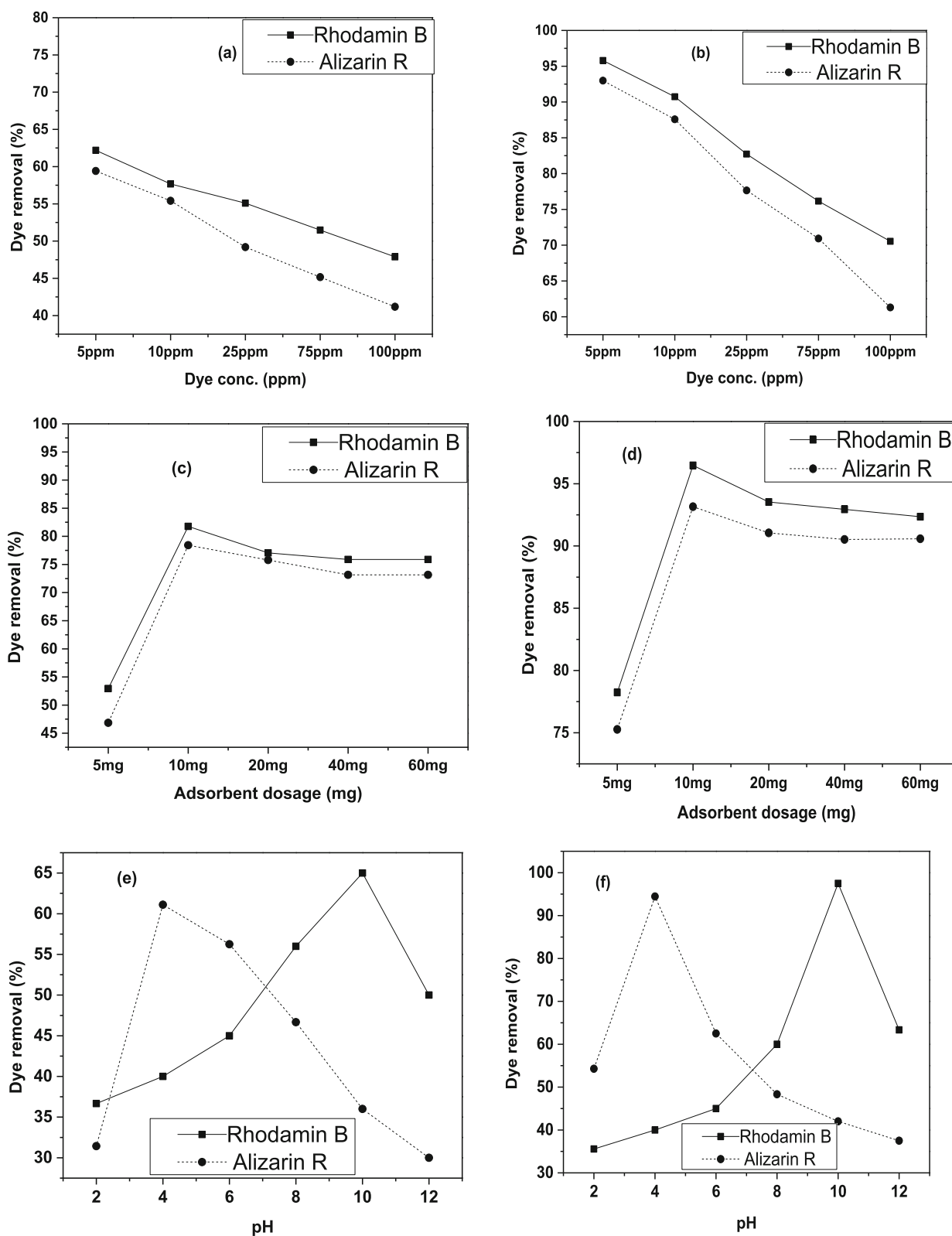


Fig. 6 Dye concentration effect on dyes removal **a** without tungsten lamp **b** under tungsten lamp, Nanocatalyst amount effect on dyes removal **c** without tungsten lamp **d** under tungsten lamp, pH effect on dyes removal **e** without tungsten lamp **f** under tungsten lamp, Temperature effect **g** without tungsten lamp **h** under tungsten lamp, Time

factor of rhodamin B dye removal **i** without tungsten lamp **j** under tungsten lamp, for alizarin R dye removal **k** without tungsten lamp **l** under tungsten lamp

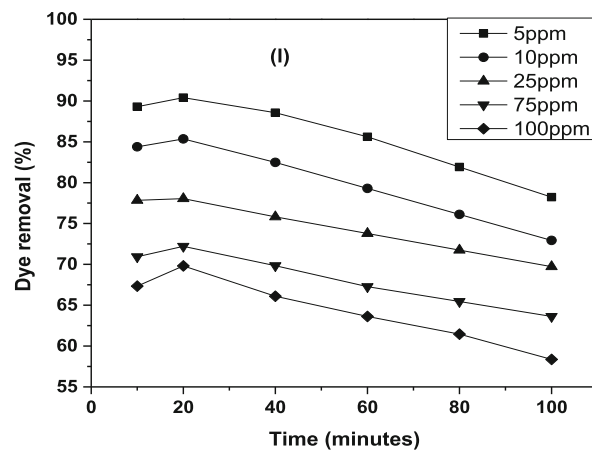
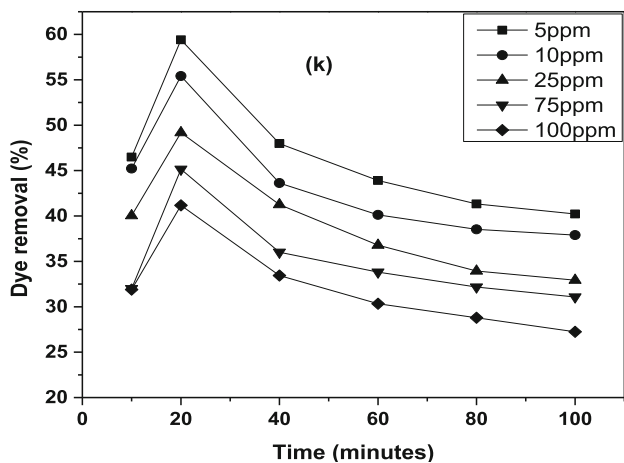
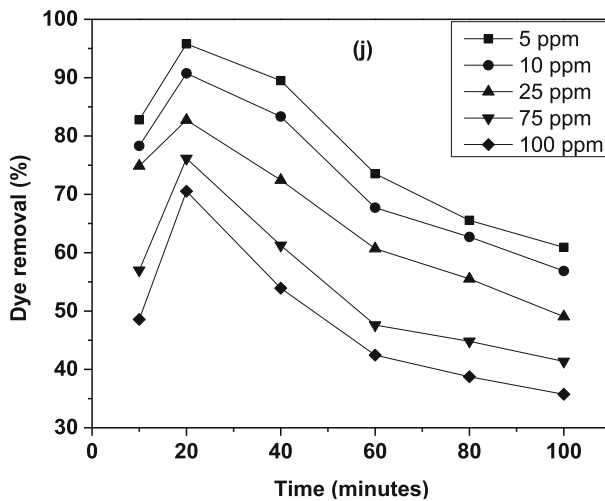
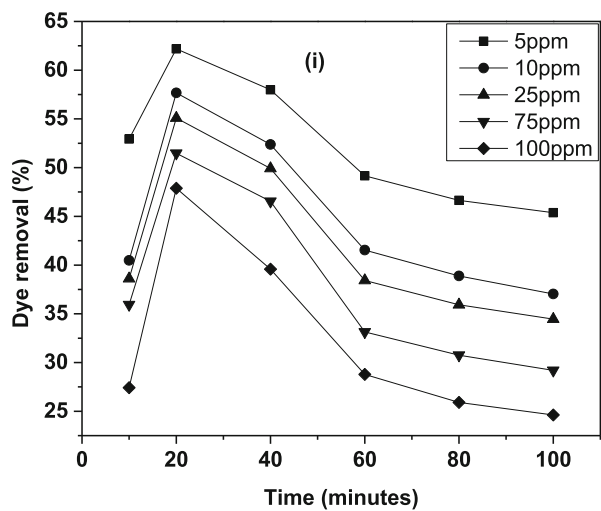
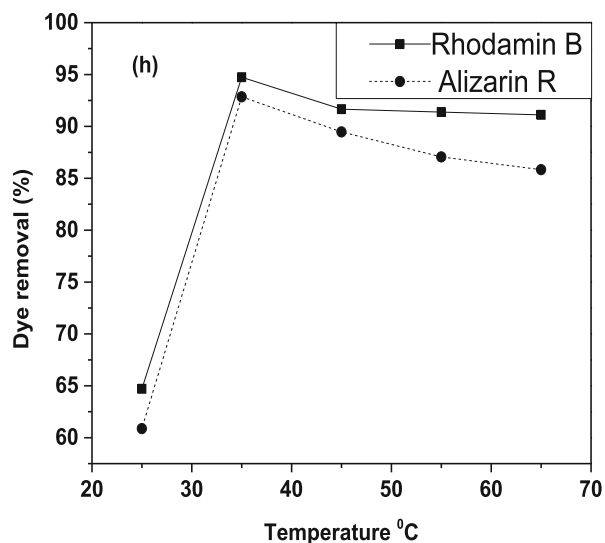
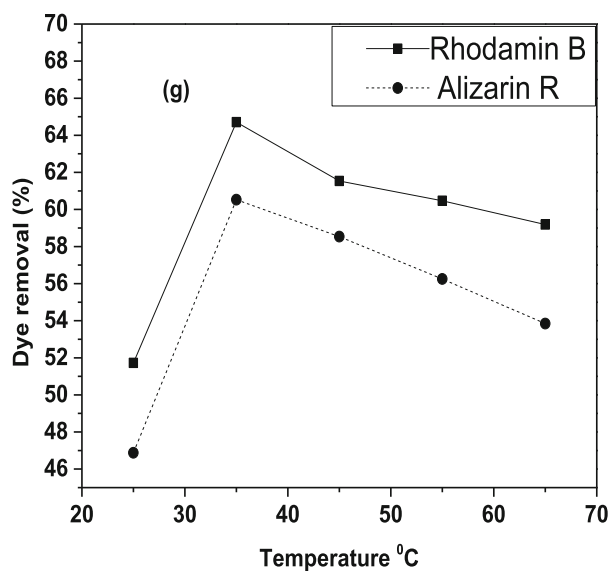


Fig. 6 continued

3.7.2 Effect of Nanocatalyst Dosage

To know about the specific amount of nanocatalyst which is required to remove dye from water nanocatalyst dosage factor was optimized. For this purpose different nanocatalyst dosages (5 mg, 10 mg, 20 mg, 40 mg and 60 mg) were added to the 25 mL binary solution of dye. 5 ppm solution was used to optimize this factor; after adding each of fixed amount of adsorbent, solution was kept at room temperature (25 °C) for 2-h stirring. From Fig. 6c and d it was seen that by increasing adsorbent dose, the % removal of dyes increased up to a certain limit. And it was noticed that after 10 mg adsorbent dosage, equilibrium was established. Actually % removal of dyes depends upon the availability of active sites of adsorbent, so when all sites were occupied, then equilibrium was established [32]. Hence, certain amount, i.e., 10 mg of adsorbent, was recorded as ideal quantity and was used for further factors optimization. 81% of rhodamine B and 78% of alizarin R were removed from binary solution of dyes without tungsten lamp, while 96% of rhodamine B and 93% of alizarin R were removed under tungsten lamp source [33, 34].

3.7.3 Effect of pH

Adsorption capacity also depends upon pH of the reaction mixture. Interaction of adsorbent with dyes at specific pH can increase the % removal of dyes. To optimize the pH factor, 2–12 pH range was adjusted. Reaction conditions were kept same throughout the process, i.e., 10 mg nanocatalyst in 25 ml binary solution of dyes at 25 °C. As shown in Fig. 6e and f, % removal of rhodamine B dye was 65% and alizarin R was 61% without using tungsten lamp, while % removal was 97% for rhodamine B dye and 94% for alizarin R dye under tungsten lamp. As rhodamine B was cationic dye, its adsorption was maximum toward negatively charged surface at higher pH value, i.e., 10. On the other hand, at lower pH value nanocatalyst surface was positively charged and anionic dye (alizarin R) attracted more toward the opposite charges; therefore, maximum removal was seen at lower pH value, i.e., 4 [35, 36].

3.7.4 Effect of Temperature

Rhodamin B and alizarin R dyes are thermally stable upto 195 °C and 100 °C. Because of their higher thermal stability, these dyes cannot degrade by itself, but treating with nanocatalyst like Fe/Co/rGO can degrade these dyes at very low temperature. To confirm the optimum temperature where maximum removal of dyes can be seen temperature range between 25 and 65 °C was set. 10 mg nanocatalyst was added into 25 ml binary solution of dyes, and % removal was observed at 25 °C, 35 °C, 45 °C, 55 °C and 65 °C. From

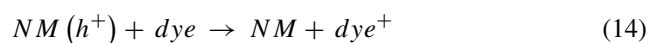
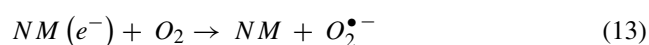
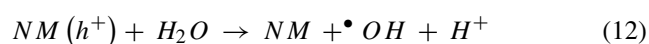
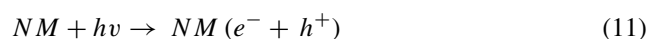
Fig. 6g and h, it was clear that by increasing temperature the % removal of dyes increased upto a specific temperature, i.e., 35 °C due to extra movement of dye molecules. Without tungsten lamp, % removal of rhodamine B was 64% and alizarin R was 60%. Same experiment was performed under tungsten lamp, and % removal was 94% and 92% for rhodamine B and alizarin R dyes, respectively [37, 38].

3.7.5 Effect of Time

Contact time is very important to observe the % removal of dyes. To analyze the contact time experiment was performed by adding 10 mg nanocatalyst in 25 ml binary solution of dyes in the time range between 10 and 100 min. It was seen that with the passage of time dye removal % age was increased due to more time of interaction of dye molecules with nanocatalyst (Fig. 6i, j, k and l). But this phenomenon was seen for a short time of 20 min until the establishment of equilibrium. Actually at start of interaction of nanocatalyst and dye molecules, more active sites were available, but with the passage of time active sites of nanocatalyst got occupied. Here in this case of Fe/Co/rGO nanocatalyst and binary solution of dyes maximum % removal of dyes was observed without tungsten lamp and under tungsten lamp. Without tungsten lamp, % removal of rhodamine B was 62% and alizarin R was 59%. Under tungsten lamp, % removal was increased upto 95% for rhodamine B and 90% for alizarin R [39, 40].

3.7.6 Photooxidation of Dyes

Natural and synthetic dyes are used in different industries for coloring. Industrial effluents containing dyes are carcinogenic and are lethal for aquatic system [41]. Dyes reduce the BOD (biological oxygen demand) and COD (chemical oxygen demand) level of water that is very harmful for aquatic living organisms as well as human beings [42]. Hence it is very necessary to degrade the dyes into nontoxic products. Adsorption mechanism is considered very best method for this purpose. Proposed mechanism of photooxidation of dyes adsorption will be like that:



Here NM indicated the nanomaterial.

Table 1 Thermodynamics parameters with and without tungsten lamp

Adsorbent	Constants	Without tungsten lamp	Under tungsten lamp		
Fe/Co/rGO		RhB	AR	RhB	AR
	Temp (K)	298	298	298	298
		308	308	308	308
		318	318	318	318
		328	328	328	328
		338	338	338	338
	K_L	2.67	2.20	4.58	3.88
		4.58	3.83	45	32.5
		5	4.37	47.5	37.08
		5.76	5	63.40	40
		6.25	5.14	87.5	57.5
	$\Delta H^\circ(\text{KJ mol}^{-1})$	16.33	16.68	53.21	47.78
	$\Delta S^\circ(\text{Jmol}^{-1} \text{K}^{-1})$	64.27	63.96	197.30	177.47
	$\Delta G^\circ(\text{KJ mol}^{-1})$	- 2.44	- 1.96	- 3.77	- 3.36
		- 3.89	- 3.44	- 9.74	- 8.91
		- 4.25	- 3.90	- 10.20	- 9.55
		- 4.77	- 4.38	- 11.31	- 10.05
		- 5.14	- 4.60	- 12.56	- 11.38
	R^2	0.81	0.77	0.64	0.61

Degradation of dyes begins when a catalytic material is exposed to a synthetic or natural light source. A hole in the valance band (VB) of the catalytic material is formed when energy of the falling light will be greater or equal than the band energy; as a result, an electron moves from valance band (VB) to the conduction band (CB). The rGO sheets serve as a trap to prevent the abrupt recombination of the electrons into the electron-hole pairs once the electrons have been transported to them. As adsorption is performed in a water-based system, oxygen adsorbs on the outer surface of the catalytic material and will act as electron acceptor. On the other hand

electron donors are hydroxyl anions and water molecules. As a result, oxidizing $\cdot\text{OH}$ radicals, oxygen and superoxide anions are formed. After adsorption of dye molecules on the catalytic material, powerful oxidizing $\cdot\text{OH}$ radicals react with dye molecules to form different fragments and adducts and this process runs until complete degradation occurs [43, 44].

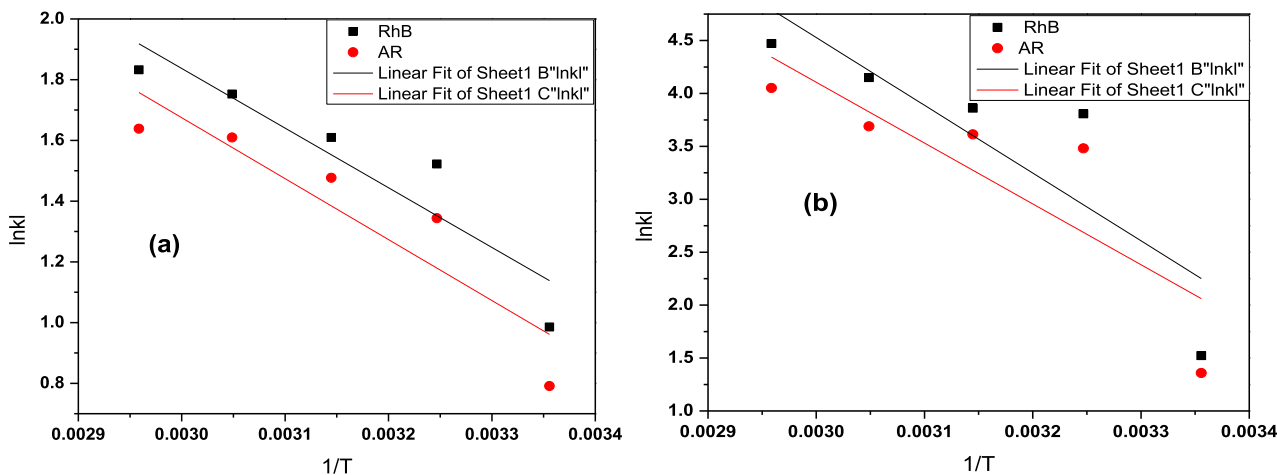


Fig. 7 Van't Hoff plots for rhodamin B and Alizarin R dyes **a** without tungsten lamp **b** under tungsten lamp

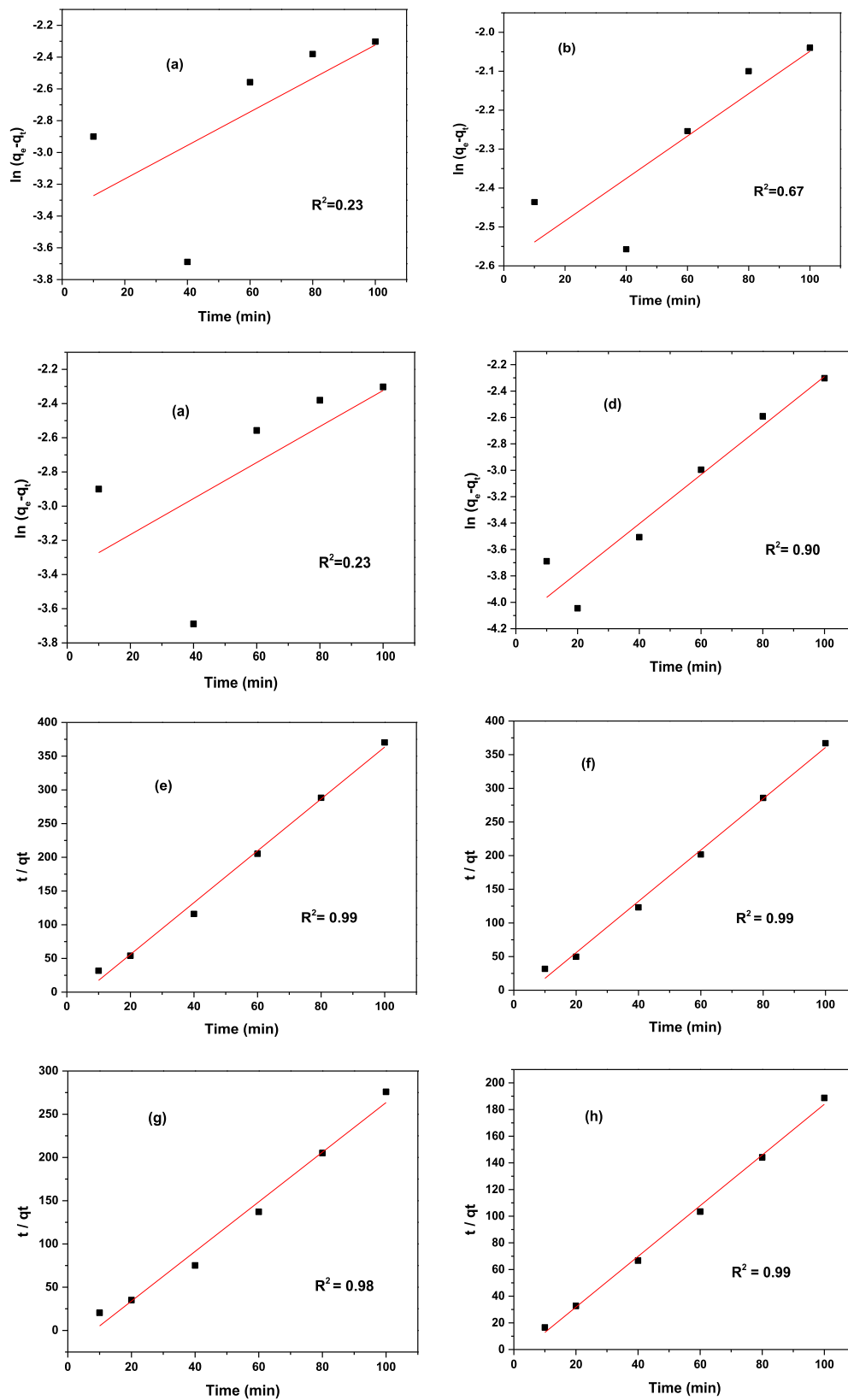


Fig. 8 Pseudo 1st order for rhodamin B **a** without tungsten lamp **c** under tungsten lamp and for alizarin R dye **b** without tungsten lamp **d** under tungsten lamp, Pseudo 2nd order for rhodamin B **e** without tungsten

lamp **g** under tungsten lamp and alizarin R dye **f** without tungsten lamp **h** under tungsten lamp

Table 2 Parameters of kinetics of adsorption for rhodamin B & alizarin R dyes on Fe/Co/rGO nanocomposite

Kinetics models	Constants	Under tungsten lamp		Without tungsten lamp	
		RhB dye	AR dye	RhB dye	AR dye
Pseudo 1st order	K_1 (min^{-1})	0.0001517	0.0001859	0.0001054	0.0000545
	q_e	0.044605	0.015786	0.034144	0.074769
	R^2	0.43163	0.90945	0.23266	0.67175
Pseudo 2nd order	K_2 (min^{-1})	-0.00728	-0.17861	-0.00321	-0.00552
	q_e	0.3525	0.576349	0.260064	0.26628
	R^2	0.99327	0.99981	0.99223	0.9985

3.8 Thermodynamics Parameters

By plotting graph between $1/T$ and $\ln K_d$, intercept and slope values were taken to calculate thermodynamic parameters, i.e., ΔH , ΔG° and ΔS° (Table 1). Negative value of ΔG° indicated the spontaneous reaction of adsorption. It was observed that negative value of ΔG° increased with increasing temperature and thus high temperature favored the reaction as shown in Fig. 7. Entropy and enthalpy showed the positive values which were the indicator of exothermic reaction and more randomness, respectively. Increase in temperature enhanced the kinetic energy of molecules, and thus, randomness favored the adsorption reaction [45].

3.9 Adsorption Kinetics Models

In PFO rate-limiting step and adsorption rate depended upon the concentration of adsorbate; therefore, this model was controlled by physisorption, while in PSO model adsorption was considered to be controlled by chemisorption [46].

Adsorption kinetics models were utilized to analyze the interaction process of adsorbent with adsorbate and reaction time. Values of these constants can be calculated by plotting graphs between $\ln(q_e - q_t)$ and time (t) in PFO and plot between $\frac{t}{q_t}$ and time (t) in PSO (Fig. 8). From slope and intercept of straight line plots values were calculated and are given in Table 2. Best fitted model was PSO for adsorption mechanism of dyes on synthesized nanocatalyst as R^2 value for both dyes was near to unity.

3.9.1 Adsorption Isotherms

Adsorption isotherms were used to predict the interaction of dye molecules with nanocatalyst [47]. The graphs for Langmuir, Freundlich and Temkin isotherm are given in Fig. 9. The best fitted model was Freundlich isotherm from R^2 value which was near to 1 during all experiments of adsorption performed without tungsten lamp and under tungsten lamp. Low value of $1/n$ predicted the heterogeneous surface of nanocatalyst which is very suitable for adsorption mechanism. Hence

all constants of Freundlich equation favor the adsorption of dye molecules on nanocatalyst.

On the other hand, Langmuir adsorption isotherm predicted the homogeneous nature of adsorbent surface and unilayer formation of dye molecules on nanocatalyst. Higher value of q_m indicated maximum monolayer formation. R_L is affinity parameter of Langmuir isotherm, and its low value favored the adsorption.

In Temkin model greater value of B_T than "0" indicated the exothermic nature of adsorption process. All calculated values of these isotherms are given in Table 3.

3.10 Reusability of Synthesized Nanocomposite

It is also a serious issue to discard solid waste material after adsorption of dyes on adsorbent. Many researchers are working on this environmental threat. The adsorbing material can be regenerated to make it less toxic to the environment [48]. In this work cationic and anionic dyes were considered, and thus, both acidic pH and basic pH were important during adsorption process as shown in Fig. 10a and b. For the desorption of rhodamine B (cationic dye) from adsorbing material Fe/Co/rGO HCl solution of 0.01 M was used, and for alizarin R (anionic dye), NaOH solution of 0.01 M was used. After desorption of dyes adsorbent can be reused 5 times, but efficiency was gradually decreased upto 76%.

3.11 Interferences of Ions

Adsorption capacity of synthesized composite Fe/Co/rGO was not much affected by interfering ions. Actually different additives can be present in industrial water and can speed up or depress the reaction of nanocatalyst with dye molecules [49]. To analyze the effect of different ions like surfactants and salts, three salt solutions (NaNO_3 , NaCl , Na_2CO_3) were used. Salt solutions of 0.1 M and dyes (25 ml of 5 ppm) were prepared, and an optimized amount of adsorbent, i.e., 10 mg, was added into 3 separate beakers. Reaction was allowed for 1 h on orbital shaker, and results are given in Fig. 10c



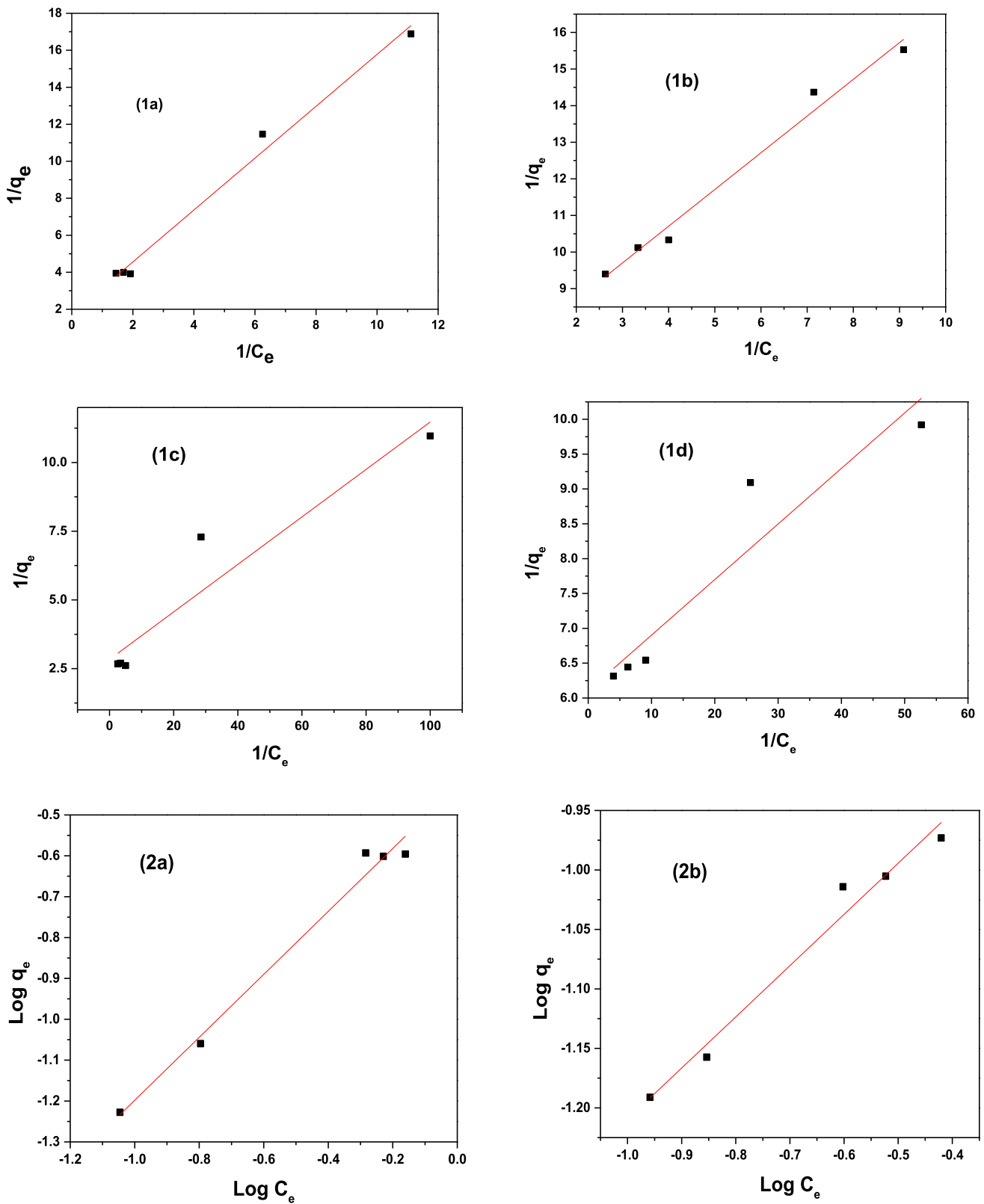


Fig. 9 Langmuir isotherm for rhodamin B **1a** without tungsten lamp **1b** under tungsten lamp, for alizarin R **1c** without tungsten lamp **1d** under tungsten lamp, Freundlich isotherm for rhodamin B **2a** without tungsten lamp **2b** under tungsten lamp for alizarin R **2c** without tungsten lamp **2d**

under tungsten laemkin isotherm for rhodamin B **3a** without tungsten lamp **3b** under tungsten lamp for alizarin R **3c** without tungsten lamp **3d** under tungsten lamp

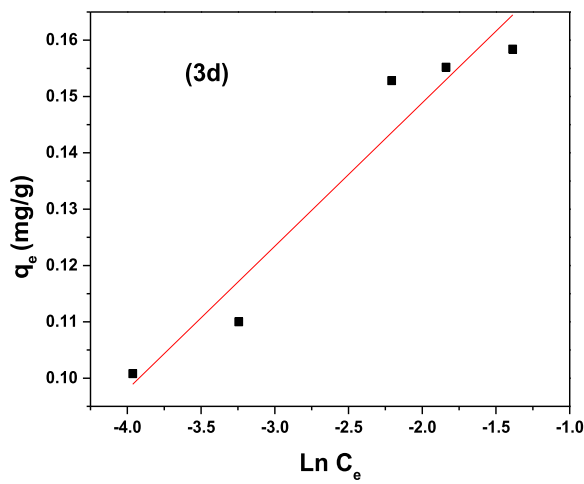
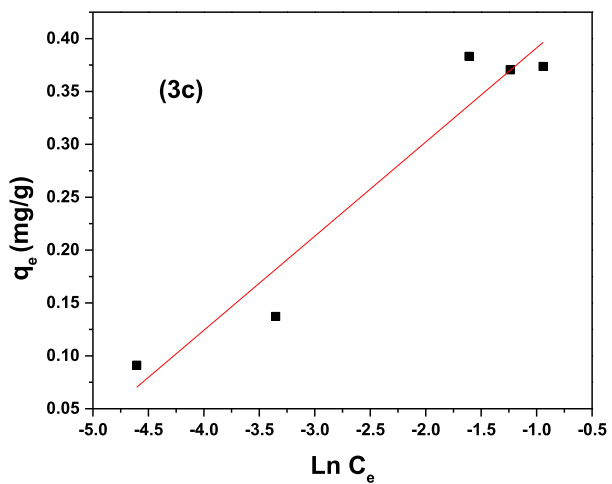
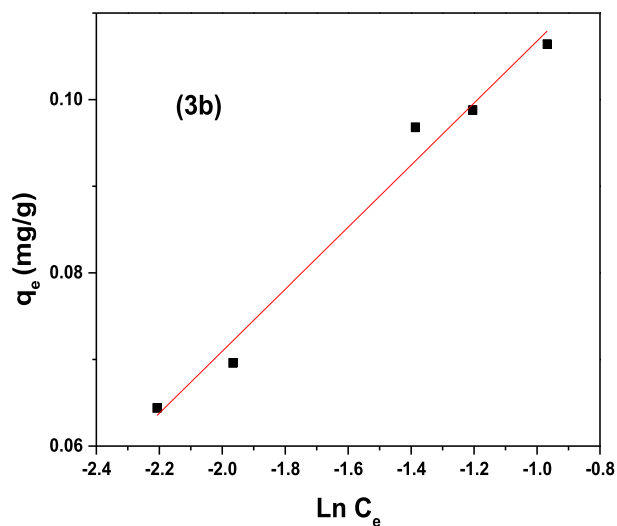
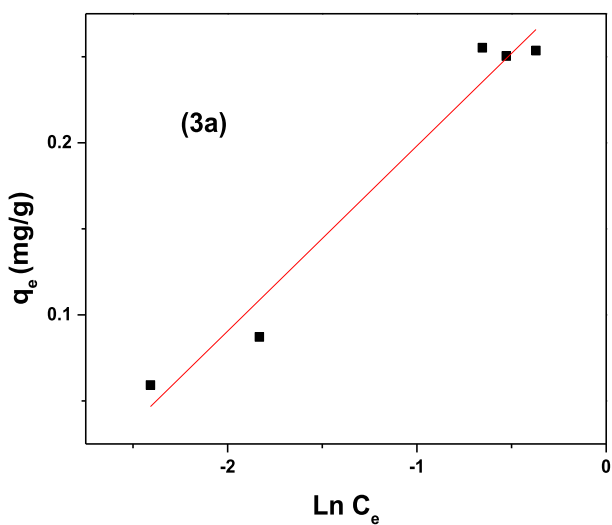
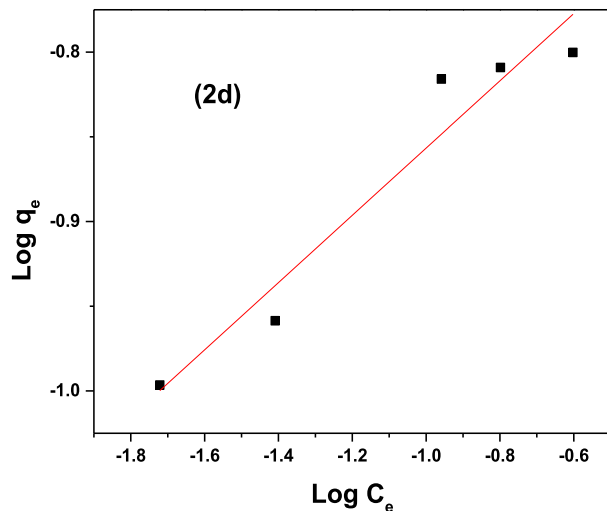
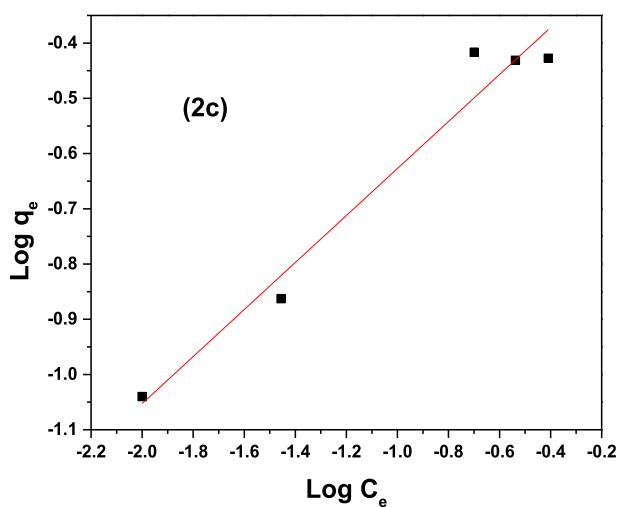


Fig. 9 continued

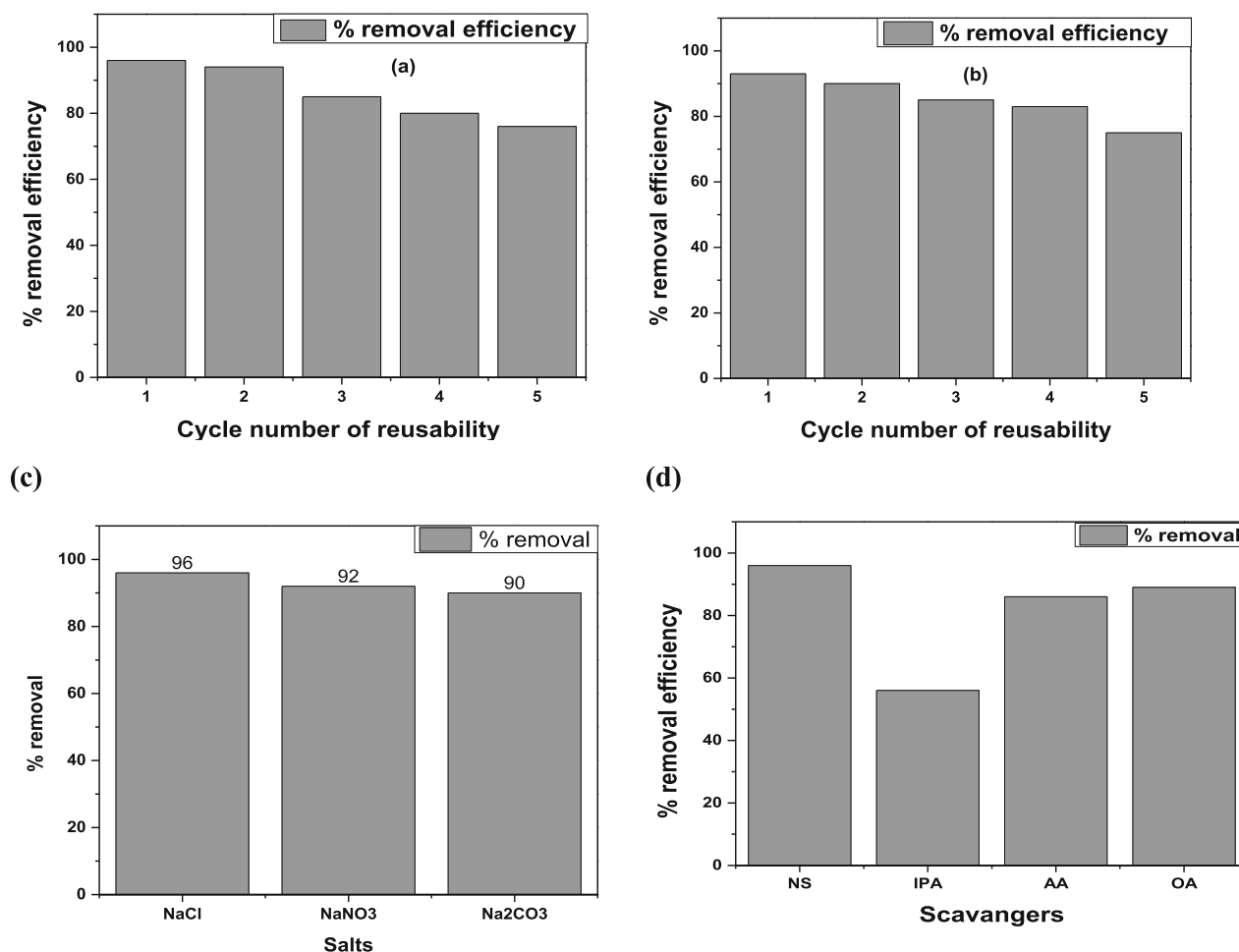


Fig. 10 Reusability of Fe/Co/rGO composite **a** rhodamin B dye and **b** alizarin R **c** Interferences of ions on adsorption capacity of Fe/Co/rGO composite **d** Effect of scavengers on dyes removal

which showed interfering ions have not any marked effect on removal of dyes by nanocomposite.

3.11.1 Scavengers Effect on Degradation Mechanism

Isopropyl alcohol (IPA) for hydroxyl radicals, oxalic acid (OA) for holes scavengers and ascorbic acid (AA) for superoxides were used to analyze the effect of reactive specie involved during adsorption mechanism. Results with these three scavengers and without any scavenger are given in Fig. 10d. By comparing the results, it can be seen that % removal efficiency was 96% without any scavenger for both dyes and hydroxyl radical was the main specie that involved in the photocatalytic degradation mechanism [50, 51]. Isopropyl alcohol was the only one scavenger that played an important role during degradation mechanism and % removal efficiency was reduced upto 56%, while oxalic acid and ascorbic acid played a very little role and % removal efficiency was observed as 89% and 86%.

4 Conclusion

In this research work, photocatalytic material Fe/Co/rGO was synthesized by using aqueous extract of *Dypsis lutescens* in a single step. Constituents of the plant acted as reducing and stabilizing agents during formation of nanocomposite. Synthesis of nanocomposite was confirmed by UV-visible spectrophotometer, FTIR, XRD, EDX and SEM which showed the porous and crystalline structure with average size of 5 nm. Synthesized photocatalyst was used to remove cationic dye (Rhodamine B) and anionic dye (Alizarin R) from their mixture solution by optimizing different factors. The best conditions were concluded as 10 mg adsorbent dosage with maximum time of 20 min at 35 °C exhibited efficient removal of dyes in a single step with and without aid of tungsten lamp. Thermodynamics study revealed the excellent affinity of dyes' molecules with nanocatalyst, spontaneity of the reaction and endothermic nature. From adsorption kinetics models, it was concluded that pseudo-2nd order was the

Table 3 Calculated parameters of adsorption isotherms for rhodamin B & alizarin R dyes on Fe/Co/rGO nanocomposite

Isothermss	Constants	Without tungsten lamp		Under tungsten lamp	
		RhB	AR	RhB	AR
Freundlich isotherm	Intercept	− 0.42	− 0.77	− 0.20	− 0.65
	Slope	0.77	0.43	0.42	0.19
	1/n	0.77	0.43	0.42	0.19
	K _f	0.37	0.16	0.62	0.21
	R ²	0.98	0.97	0.95	0.92
Langmuir isotherm	Intercept	1.75	6.69	2.83	6.10
	Slope	1.40	1.003	0.08	0.07
	K _L (L/g)	1.24	0.14	32.84	2.05
	q _m (mg/g)	0.57	0.14	0.35	0.16
	R _L	0.13	0.16	0.025	0.12
Temkin isotherm	R ²	0.98	0.97	0.88	0.86
	Slope	0.10	0.03	0.08	0.02
	BT (J mol ^{−1})	0.10	0.03	0.08	0.02
	Kr (L mg ^{−1})	17.14	53.55	220.18	2.19
	R ²	0.96	0.97	0.91	0.92

best fitted method for adsorption mechanism. Three adsorption isotherms were applied to select the best fitted model and among them Freundlich isotherm found as best. Adsorption capacity was not interrupted with different ions. The synthesized nanocomposite Fe/Co/rGO was reused upto 5 times with slight difference of removal capacity. During adsorption mechanism, hydroxyl radicals were the main reactive specie as determined by scavengers effect experiment.

Declarations

Conflict of interest The authors declare no conflict of interest. The authors declare that they have no known competing financial interests or personal relationships that could have appeared to influence the work reported in this paper.

References

- Jinendra, U.; Bilehal, D.; Nagabhushana, B.; Kumar, A.P.: Adsorptive removal of Rhodamine B dye from aqueous solution by using graphene-based nickel nanocomposite. *Heliyon*. **7**(4), e06851 (2021). <https://doi.org/10.1016/j.heliyon.2021.e06851>
- Rajasulochana, P.; Preethy, V.: Comparison on efficiency of various techniques in treatment of waste and sewage water—a comprehensive review. *Resour. Effic. Tech.* **2**(4), 175–184 (2016). <https://doi.org/10.1016/j.refit.2016.09.004>
- Wang, C.; Cheng, F.; Ma, X.; Wu, Q.: Preparation of a graphene-based magnetic nanocomposite for the removal of an organic dye from aqueous solution. *Chem. Eng. J.* **173**(1), 92–97 (2011). <https://doi.org/10.1016/j.cej.2011.07.041>
- Chen, H.; Zhu, S.; Zhang, D.; Xu, S.: Synthesis and properties of magnetic Fe₃O₄-activated carbon nanocomposite particles for dye removal. *Mater. Lett.* **62**(4–5), 645–647 (2008). <https://doi.org/10.1016/j.matlet.2007.06.049>
- Ambashta, R.D.; Sillanpää, M.: Water purification using magnetic assistance: a review. *J. Hazard. Mater.* **180**(1–3), 38–49 (2010). <https://doi.org/10.1016/j.jhazmat.2010.04.105>
- Chen, J.; Wang, X.; Huang, Y.; Lv, S.; Cao, X.; Yun, J.; Cao, D.: Adsorption removal of pollutant dyes in wastewater by nitrogen-doped porous carbons derived from natural leaves. *Eng. Sci.* **5**, 30–38 (2018). <https://doi.org/10.30919/es8d666>
- Neelgund, G.M.; Oki, A.: Folic acid and CuS conjugated graphene oxide: an efficient photocatalyst for explicit degradation of toxic dyes. *Appl. Surf. Sci.* **566**, 150648 (2021). <https://doi.org/10.1016/j.apsusc.2021.150648>
- Katheresan, V.; Kansedo, J.; Lau, S.Y.: Efficiency of various recent wastewater dye removal methods: a review. *J. Environ. Chem. Eng.* **6**(4), 4676–4697 (2018). <https://doi.org/10.1016/j.jece.2018.06.060>
- Singh, K.; Arora, S.: Removal of synthetic textile dyes from wastewaters: a critical review on present treatment technologies. *Crit. Rev. Environ. Sci. Technol.* **41**(9), 807–878 (2011). <https://doi.org/10.1080/10643380903218376>
- Bhatia, D.S.; Sharma, N.; Singh, J.; Kanwar, R.S.: Biological methods for textile dye removal from wastewater: a review. *Crit. Rev. Environ. Sci. Technol.* **47**(19), 1836–1876 (2017). <https://doi.org/10.1080/10643389.2017.1393263>
- Santhy, K.; Selvapathy, P.: Removal of reactive dyes from wastewater by adsorption on coir pith activated carbon. *Bioresour. Technol.* **97**(11), 1329–1336 (2006). <https://doi.org/10.1016/j.biortech.2005.05.016>
- Yagub, M.T.; Sen, T.K.; Afroze, S.; Ang, H.M.: Dye and its removal from aqueous solution by adsorption: a review. *Adv. Colloid Interface Sci.* **209**, 172–184 (2014). <https://doi.org/10.1016/j.cis.2014.04.002>
- Liu, J.; Ma, Q.; Huang, Z.; Liu, G.; Zhang, H.: Recent progress in graphene-based noble-metal nanocomposites for electrocatalytic applications. *Adv. Mat.* (2018). <https://doi.org/10.1002/adma.201800696>



14. Khan, M.; Tahir, M.N.; Adil, S.F.; Khan, H.U.; Al-Warthan, A.; Tremel, W.: Graphene based metal and metal oxide nanocomposites: synthesis, properties and their applications. *J. Mat. Chem. A* **3**(37), 18753–18808 (2015). <https://doi.org/10.1039/c5ta02240a>
15. El-Ghonemy, M.M.; El-Kashak, W.A.; Mohamed, T.K.; Omara, E.A.; Hussein, J.; Farrag, A.R.H.; El-Kady, M.Y.: Hepatoprotective activity of *Dypsislutescens* against D-galactosamine-induced hepatotoxicity in rats and its phytoconstituents. *Asian Pac. J. Trop. Biomed.* **9**(11), 467 (2019)
16. Nasrollahzadeh, M.; Sajjadi, M.; Komber, H.; Khonakdar, H.A.; Sajadi, S.M.: In situ green synthesis of Cu-Ni bimetallic nanoparticles supported on reduced graphene oxide as an effective and recyclable catalyst for the synthesis of N-benzyl-N-aryl-5-amino-1H-tetrazoles. *Appl. Organomet. Chem.* (2019). <https://doi.org/10.1002/aoc.4938>
17. Ji, C.; Yao, B.; Li, C.; Shi, G.: An improved Hummers method for eco-friendly synthesis of graphene oxide. *Carbon* **64**, 225–229 (2013). <https://doi.org/10.1016/j.carbon.2013.07.055>
18. Zaaba, N.I.; Foo, K.L.; Hashim, U.; Tan, S.J.; Liu, W.; Voon, C.H.: Synthesis of graphene oxide using modified hummers method: solvent influence. *Procedia Eng.* **184**, 469–477 (2017). <https://doi.org/10.1016/j.proeng.2017.04.118>
19. Cao, N.; Zhang, Y.: Study of reduced graphene oxide preparation by Hummers' method and related characterization. *J. Nanomat.* (2015). <https://doi.org/10.1155/2015/168125>
20. Kanwal, A.; Shahzadi, T.; Riaz, T.; Zaib, M.; Khan, S.; Habila, M.A.; Sillanpaa, M.: Photocatalytic degradation studies of organic dyes over novel Cu/Ni loaded reduced graphene oxide hybrid nanocomposite: adsorption. *Kinet. Thermodyn. Stud. Mol.* **28**(18), 6474 (2023)
21. Khataee, A.; Kiranşan, M.; Karaca, S.; Oskoui, S.A.: Preparation and characterization of ZnO/MMT nanocomposite for photocatalytic ozonation of a disperse dye. *Turk. J. Chem.* **40**, 546–564 (2016). <https://doi.org/10.3906/kim-1507-77>
22. Singh, S.; Khasnabis, S.; Anil, A.G.; Kumar, V.; Naik, T.S.K.; Nath, B.; Garg, V.; Singh, J.: Multifunctional nanohybrid for simultaneous detection and removal of Arsenic (III) from aqueous solutions. *Chemosphere* **289**, 133101 (2022). <https://doi.org/10.1016/j.chemosphere.2021.133101>
23. Keshvardoostchokami, M.; Piri, F.; Zamani, A.: One-pot synthesis of chitosan/iron oxide nanocomposite as an eco-friendly bioadsorbent for water remediation of methylene blue. *Micro. Nano. Lett.* **12**(5), 338–343 (2017). <https://doi.org/10.1049/mnl.2016.0681>
24. Stobinski, L.; Lesiak, B.; Malolepszy, A.; Mazurkiewicz, M.; Mierzwa, B.; Zemek, J.; Jiricek, P.; Bieloshapka, I.: Graphene oxide and reduced graphene oxide studied by the XRD, TEM and electron spectroscopy methods. *J. Elect. Spectrosc.* **195**, 145–154 (2014). <https://doi.org/10.1016/j.elspec.2014.07.003>
25. Benkhaya, B.; Harfi, S. E.; Harfi, A. E.: (2017) Classifications, properties and applications of textile dyes: a review. *Appl. J. Environ.* <https://doi.org/10.48422/imist.prs/ajees-v3i3.9681>
26. Samsami, S.; Mohamadizani, M.; Sarrafzadeh, M.; Rene, E.R.; Firoozbahr, M.: Recent advances in the treatment of dye-containing wastewater from textile industries: overview and perspectives. *Process. Saf. Environ. Prot.* **143**, 138–163 (2020). <https://doi.org/10.1016/j.psep.2020.05.034>
27. Al-Ghouti, M.A.; Khraisheh, M.; Allen, S.; Ahmad, M.: The removal of dyes from textile wastewater: a study of the physical characteristics and adsorption mechanisms of diatomaceous earth. *J. Environ. Manage.* **69**(3), 229–238 (2003). <https://doi.org/10.1016/j.jenvman.2003.09.005>
28. Hayati, B.; Mahmoodi, N.M.: Modification of activated carbon by the alkaline treatment to remove the dyes from wastewater: mechanism, isotherm and kinetic. *Desal. Water Treat.* **47**(1–3), 322–333 (2012). <https://doi.org/10.1080/19443994.2012.696429>
29. Dutta, S.; Gupta, B.R.; Srivastava, S.K.; Gupta, A.K.: Recent advances on the removal of dyes from wastewater using various adsorbents: a critical review. *Mater. Advan.* **2**(14), 4497–4531 (2021). <https://doi.org/10.1039/d1ma00354b>
30. Shahzadi, T.; Kanwal, A.; Jabeen, H.; Riaz, T.; Zaib, M.: Eco-friendly synthesis of silver nanoparticles using *Gazania rigens* and evaluation of activities. *Environ. Engin. Manag. J.* **20**(1), 43–52 (2021)
31. Shahzadi, T.; Rehman, S.; Riaz, T.; Zaib, M.: Eco-friendly synthesis of ZnO nanoparticles using *Cannabis sativa* and assessment of its activities as efficient dyes removal and antioxidant agent. *Int. J. Environ. Anal. Chem.* **102**(16), 4738–4756 (2020). <https://doi.org/10.1080/03067319.2020.1789610>
32. Shahzadi, T.; Sanaullah, S.; Riaz, T.; Zaib, M.; Kanwal, A.; Jabeen, H.: Kinetics and thermodynamic studies of organic dyes removal on adsorbent developed from Viola tricolor extract and evaluation of their antioxidant activity. *Environ. Dev. Sustain.* **23**(12), 17923–17941 (2021). <https://doi.org/10.1007/s10668-021-01421-0>
33. Pirsaeheb, M.; Moradi, N.: A systematic review of the sonophotocatalytic process for the decolorization of dyes in aqueous solution: synergistic mechanisms, degradation pathways, and process optimization. *J. Water Process Engin.* **44**, 102314 (2021). <https://doi.org/10.1016/j.jwpe.2021.102314>
34. Sajjad, A.K.L.; Shamaila, S.; Tian, B.; Chen, F.; Zhang, J.: Comparative studies of operational parameters of degradation of azo dyes in visible light by highly efficient WO_x/TiO₂ photocatalyst. *J. Hazard. Mat.* **177**(1–3), 781–791 (2010). <https://doi.org/10.1016/j.jhazmat.2009.12.102>
35. Mahmoodi, N.M.; Keshavarzi, S.; Ghezalbash, M.: Synthesis of nanoparticle and modelling of its photocatalytic dye degradation ability from colored wastewater. *J. Environ. Chem. Eng.* **5**(4), 3684–3689 (2017). <https://doi.org/10.1016/j.jece.2017.07.010>
36. Zulmajdi, S.L.N.; Zamri, N.I.I.; Yasin, H.M.; Kusri, E.; Hobbey, J.; Usman, A.: Comparative study on the adsorption, kinetics, and thermodynamics of the photocatalytic degradation of six different synthetic dyes on TiO₂ nanoparticles. *React. Kinet. Mech. Catal.* **129**(1), 519–534 (2019). <https://doi.org/10.1007/s11144-019-01701-x>
37. Nguyen, D.T.C.; Le, H.T.; Nguyen, T.T.; Nguyen, T.T.; Bach, L.G.; Nguyen, T.D.; Van Tran, T.: Multifunctional ZnO nanoparticles bio-fabricated from *Canna indica* L. flowers for seed germination, adsorption, and photocatalytic degradation of organic dyes. *J. Hazard. Mat.* (2021). <https://doi.org/10.1016/j.jhazmat.2021.126586>
38. Singh, R.K.; Behera, S.S.; Singh, K.; Mishra, S.; Panigrahi, B.; Sahoo, T.R.; Parhi, P.K.; Mandal, D.: Biosynthesized gold nanoparticles as photocatalysts for selective degradation of cationic dye and their antimicrobial activity. *J. Photochem. Photobio. A: Chem.* **400**, 112704 (2020). <https://doi.org/10.1016/j.jphotochem.2020.112704>
39. Nguyen, D.T.C.; Le, H.T.; Nguyen, T.T.; Nguyen, T.T.; Bach, L.G.; Nguyen, T.D.; Van Tran, T.: Multifunctional ZnO nanoparticles bio-fabricated from *Canna indica* L. flowers for seed germination, adsorption, and photocatalytic degradation of organic dyes. *J. Hazard. Mat.* **420**, 126586 (2021). <https://doi.org/10.1016/j.jhazmat.2021.126586>
40. Peng, X.; Zhang, W.; Gai, L.; Jiang, H.; Wang, Y.; Zhao, L.: Dedoped Fe₃O₄/PPY nanocomposite with high anti-interfering ability for effective separation of Ag(I) from mixed metal-ion solution. *Chem. Engin. J.* **280**, 197–205 (2015). <https://doi.org/10.1016/j.cej.2015.05.118>
41. Lizama, C.; Freer, J.; Baeza, J.; Mansilla, H.D.: Optimized photodegradation of reactive Blue 19 on TiO₂ and ZnO suspensions. *Catal. Today* **76**(2–4), 235–246 (2002). [https://doi.org/10.1016/S0920-5861\(02\)00222-5](https://doi.org/10.1016/S0920-5861(02)00222-5)

42. Debnath, S.; Ballav, N.; Nyoni, H.; Maity, A.; Pillay, K.: Optimization and mechanism elucidation of the catalytic photo-degradation of the dyes Eosin Yellow (EY) and Naphthol blue black (NBB) by a polyaniline-coated titanium dioxide nanocomposite. *Appl. Catal. B-Environ.* **163**, 330–342 (2015). <https://doi.org/10.1016/j.apcatb.2014.08.011>
43. Akpan, U.; Hameed, B.: Parameters affecting the photocatalytic degradation of dyes using TiO₂-based photocatalysts: a review. *J. Hazard. Mat.* **170**(2–3), 520–529 (2009). <https://doi.org/10.1016/j.jhazmat.2009.05.039>
44. Zhou, F.; Yan, C.; Liang, T.; Sun, Q.; Wang, H.: Photocatalytic degradation of orange G using sepiolite-TiO₂ nanocomposites: optimization of physicochemical parameters and kinetics studies. *Chem. Engin. Sci.* **183**, 231–239 (2018). <https://doi.org/10.1016/j.ces.2018.03.016>
45. Mandel, K.; Hutter, F.; Gellermann, C.; SEXTL, G.: Reusable superparamagnetic nanocomposite particles for magnetic separation of iron hydroxide precipitates to remove and recover heavy metal ions from aqueous solutions. *Sep. Purif. Tech.* **109**, 144–147 (2013). <https://doi.org/10.1016/j.seppur.2013.03.002>
46. Monga, D.; Basu, S.: Enhanced photocatalytic degradation of industrial dye by g-C₃N₄/TiO₂ nanocomposite: role of shape of TiO₂. *Adv. Powder Tech.* **30**(5), 1089–1098 (2019). <https://doi.org/10.1016/j.apt.2019.03.004>
47. Zaib, M.; Arshad, A.; Khalid, S.; Shahzadi, T.: One pot ultrasonic plant mediated green synthesis of carbon dots and their application invisible light induced dye photocatalytic studies: a kinetic approach. *Inter. J. Environ. Ana. Chem.* **103**(17), 5063–5081 (2023). <https://doi.org/10.1080/03067319.2021.1934463>
48. Chen, F.; Xi, P.; Ma, C.; Shao, C.; Wang, J.; Wang, S.; Zeng, Z.: In situ preparation, characterization, magnetic and catalytic studies of surfactant free RGO/FexCo100–x nanocomposites. *Dalton Trans.* **42**(22), 7936–7942 (2013)
49. Riaz, T.; Asghar, A.; Shahzadi, T.; Shahid, S.; Mansoor, S.; Asghar, A.; Elkaeed, E.B.: Green synthesis of ZnO and Co-ZnO using Brassica rapa leave's extract and their activities as antioxidant agents, efficient adsorbents, and dye removal agents. *J. Saudi Chem. Soc.* **27**(5), 101716 (2023). <https://doi.org/10.1016/j.jscs.2023.101716>
50. Wang, S.; Xu, Y.; Fu, R.; Zhu, H.; Jiao, Q.; Feng, T.; Zhao, Y.: Rational construction of hierarchically porous Fe–Co/N-doped carbon/rGO composites for broadband microwave absorption. *Nano-Micro Lett.* **11**, 1–16 (2019)
51. Vijayalakshmi, S.; Elanthamilan, E.; Merlin, J.P.; Lydia, I.S.: Tuning the efficiency of CoFe₂O₄@ rGO composite by encapsulating Ag nanoparticles for the photocatalytic degradation of methyl violet dye and energy storage systems. *New J. Chem.* **45**(37), 17642–17653 (2021)

Springer Nature or its licensor (e.g. a society or other partner) holds exclusive rights to this article under a publishing agreement with the author(s) or other rightsholder(s); author self-archiving of the accepted manuscript version of this article is solely governed by the terms of such publishing agreement and applicable law.

